Phonon drag thermal Hall effect in metallic strontium titanate

Shan Jiang, Xiaokang Li, Benoît Fauqué, Kamran Behnia

Phonon drag thermal Hall effect in metallic strontium titanate

Shan Jiang,[1] Xiaokang Li,[1] Benoît Fauqué,[2] and Kamran Behnia[1]

[1] *Laboratoire de Physique et d'Étude des Matériaux (ESPCI Paris - CNRS - Sorbonne Université), PSL University, 75005 Paris, France*

[2] *JEIP, USR 3573 CNRS, Collège de France, PSL University, 75231 Paris Cedex 05, France*

(Dated: July 1, 2022)

$SrTiO_3$, a quantum paralectric, displays a detectable phonon thermal Hall effect (THE). Here we show that the amplitude of THE is extremely sensitive to stoichiometry. It drastically decreases upon substitution of a tiny fraction of Sr atoms with Ca, which stabilizes the ferroelectric order. It drastically increases by an even lower density of oxygen vacancies, which turn the system to a dilute metal. The enhancement in the metallic state exceeds by far the sum of the electronic and the phononic contributions. We explain this observation as an outcome of three features: i) heat is mostly transported by phonons; ii) the electronic Hall angle is extremely large; and iii) there is substantial momentum exchange between electrons and phonons. Starting from Herring's picture of phonon drag, we arrive to a quantitative account of the enhanced THE. Thus, phonon drag, hitherto detected as an amplifier of thermoelectric coefficients, can generate a purely thermal transverse response in a dilute metal with a large Hall angle. Our results reveal a hitherto unknown consequence of momentum-conserving collisions between electrons and phonons.

Introduction

The observation of thermal Hall effect (THE) in a variety of insulators [1–7] has attracted much recent attention. A transverse thermal gradient produced by a longitudinal flow of neutral carriers of heat requires a microscopic mechanism other than the Lorentz force. In strontium titanate, a non-magnetic insulator [8], the phononic origin of the THE [5, 9] is uncontested. Theoretical scenarios [10–16] have been proposed to explain how phonons can generate a transverse thermal gradient on top of the longitudinal one.

Ferroelectric transition is aborted by quantum critical fluctuations [17] in strontium titanate. The ground state of this quantum paraelectric [18] is unusually sensitive to the presence of extrinsic atoms [19–21]. $Sr_{1-x}Ca_xTiO_3$ is ferroelectric for $x > 0.002$ [19, 22]. Introducing a tiny amount of oxygen vacancies, on the other hand, makes the system metallic. With a carrier density of the order of $10^{17} cm^{-3}$: $SrTiO_{3-\delta}$ is a dilute metal with a sharp Fermi surface and a superconducting ground state [23]. Double substitution leads to $Sr_{1-x}Ca_xTiO_{3-\delta}$, a polar metal [24, 25], where superconductivity is boosted [26]. Here, we present a study of THE in Ca-substituted [insulating] and in oxygen-reduced [metallic] samples of strontium titanate. We find that the amplitude of the signal is significantly modified in both cases, but in opposite directions. In the case of Ca substitution, we find that THE is drastically reduced, confirming that stabilization of the ferroelectric order is detrimental to THE [9]. On the other hand, in $SrTiO_{3-\delta}$, the amplitude of THE not only exceeds what is found in the undoped insulator, but is also much larger than the sum of the expected electronic contribution and the phononic one. We argue that this surprising result can be understood by invoking the drag [27, 28] between electrons and phonons. In our temperature range of interest, heat is almost exclusively carried by phonons ($\kappa^{ph} \gg \kappa^{e}$) in this dilute metal. On the other hand, the phonon Hall angle is small ($\kappa^{ph}_{xy} < 10^{-3}\kappa^{ph}_{xx}$), but not the electronic Hall angle, which exceeds unity ($\sigma_{xy} > \sigma_{xx}$ at $\approx 2T$). In this context, momentum-conserving collisions between electrons and phonons can generate a transverse temperature gradient, because longitudinal momentum transferred to the electron bath will have a transverse counterpart, which ultimately generates a transverse energy flow. Starting from Herring's picture of phonon drag [27], we will show that this scenario yields a quantitative account of our experimental result.

Such a conclusion implies that phonon drag, hitherto known as an amplifier of the thermoelectric response [29], can have a purely thermal signature, mostly in the transverse channel. In this context, our result identifies a previously unknown consequence of quasi-particle hydrodynamics [30]. Momentum-conserving collisions between phonons and electrons [31] are a subject of growing interest in strongly-coupled electron-phonon systems [32, 33]. Momentum-conserving phonon-phonon collisions are also known to play a role in setting the amplitude of longitudinal thermal conductivity in Callaway's model [34].

Results

Our set-up (See Fig. 1 a) was designed to determine the electrical, thermoelectric and thermal transport coefficients of a single crystal during a single run. In insulating Ca-doped $SrTiO_3$ single crystals, we measured longitudinal and transverse thermal conductivities. In the case of metallic $SrTiO_{3-\delta}$ single crystals, we measured longitudinal and tranverse conductivities in thermal and electrical channels, as well as the Seebeck and the Nernst coefficients. In the latter case, by performing two sets of experiments one with a zero electrical current and another with a zero thermal current, we checked that the

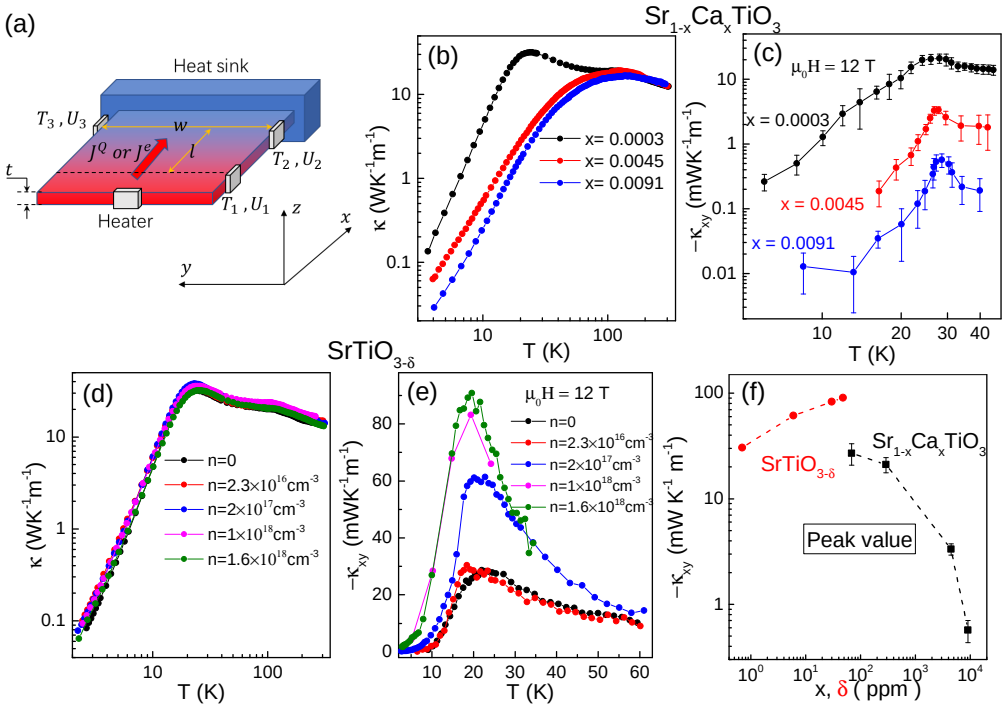

FIG. 1. **Evolution of longitudinal and transverse thermal conductivity with Ca substitution and oxygen reduction:** (a) Setup for measuring longitudinal and transverse thermal, thermoelectric and electric coefficients (the yellow pads are gold electrodes). We measured three local temperatures T_1, T_2 and T_3 and three local voltages U_1, U_2 and U_3. This allowed us to measure longitudinal and transverse temperature gradients and electric fields caused by a longitudinal heat (J^Q) or electric (J^e) current. Temperature dependence of the longitudinal, κ_{xx} (b), and transverse, κ_{xy} (c), thermal conductivity in $Sr_{1-x}Ca_xTiO_3$. The 20 K peak in κ_{xx} is wiped out. κ_{xy} decreases by almost two orders of magnitude. (d) Temperature dependence of κ_{xx} in $SrTiO_{3-\delta}$, almost unaffected by doping. (e) Temperature dependence of κ_{xy} in $SrTiO_{3-\delta}$. The amplitude enhances with oxygen substitution. (f) Amplitude of κ_{xy} peak as a function of concentration of Ca atoms (x) and O vacancies (δ) in parts per million (ppm).

transport coefficients respect Onsager reciprocity.

Calcium substitution

The evolution of longitudinal and transverse thermal conductivity with Ca substitution is shown in Fig. 1 b,c. One can clearly see that both are affected by Ca substitution. The decrease in κ_{xx} can be attributed to the random distribution of Ca atoms that introduce additional scattering. As in the case of Nb substitution [35], introducing less than a percent concentration of extrinsic atoms is sufficient to wipe out the 20 K peak of the thermal conductivity. The decrease in κ_{xy} is even more drastic. Substituting a tiny fraction (x=0.002) of Sr atoms with Ca is sufficient for stabilizing a long-range ferroelectric order [19]. This substitution eventually leads to a fifty-fold decrease in the magnitude of κ_{xy}.

A previous study on the effect of ^{18}O substitution on the thermal Hall effect in strontium titanate [9] found a decrease of comparable magnitude. Substituting Sr by Ca [24, 26] and substituting ^{16}O with ^{18}O [21, 36] both stabilize the ferroelectric order, modify the superconducting dome and generate a polar metal. In both cases, the large κ_{xy} of the quantum paraelectric solid is drastically suppressed with the stabilization of the ferroelectric order. This suggests a link between the amplitude of κ_{xy} and the presence of ferroelectric fluctuations [11]. Note that in ^{18}O-enriched strontium titanate [9], most ^{16}O atoms were substituted and the 20 K peak in κ_{xx} is still present, in contrast to what is seen here. Yet, κ_{xy} was similarly damped, ruling out that κ_{xy} is simply more sensitive to disorder.

Oxygen reduction

We investigated the effect of oxygen vacancies on THE by studying thermal transport in $SrTiO_{3-\delta}$. Fig. 1d,e shows how the temperature dependence of longitudinal and transverse thermal conductivity in $SrTiO_{3-\delta}$. The magnitude of longitudinal κ_{xx} barely changes with oxygen reduction. Assuming that each vacancy introduces two electrons, the concentration of vacancies for $n = 1.6 \times 10^{18} cm^{-3}$ (determined by measuring its Hall resitivity) is only $\delta = 4.8 \times 10^{-5}$ per formula unit, much lower than the lowest amount of Ca substitution (x= 4.5×10^{-3}). By measuring the electric conductivity

and using the Wiedemann-Franz (WF) law, we estimated the amplitude of the electronic heat conductivity. κ^e remains less than 10^{-2} of the total thermal conductivity. Therefore, thermal conductivity near the peak is not significantly reduced by disorder or enhanced by the addition of a finite electronic contribution. In contrast, κ_{xy} significantly increases with increasing n. Let us compare this enhancement with the expected electronic contribution.

Fig. 2a compares the field dependence of κ_{xy} in different samples at 20 K (i.e. near its peak). In the sample with the lowest carrier concentration ($n = 2.3 \times 10^{16} cm^{-3}$), the amplitude of κ_{xy} is almost identical to the insulating sample and remains linear in magnetic field. In samples with higher carrier concentration, the amplitude of κ_{xy} is larger and shows a gradual trend towards high-field saturation. Fig. 2b shows the electronic contribution to THE (estimated from the measured electric Hall conductivity of the metallic samples: $\kappa^e_{xy} = L_0 \sigma_{xy} T$). It shows a field-induced saturation similar to what is observed in κ_{xy}. However, subtracting the purely phononic component (taken to be equal to what is observed in the insulator) and the purely electronic component (estimated from the WF law) from the total κ_{xy} leaves us with an additional $\Delta\kappa_{xy} = \kappa_{xy} - \kappa^{ph}_{xy} - \kappa^e_{xy}$. Fig. 2d shows the temperature dependence of the different components of THE in the sample with the highest carrier concentration ($n = 1.6 \times 10^{18} cm^{-3}$). One can see that $\Delta\kappa_{xy}$ exceeds κ^{ph}_{xy} and is several times larger than κ^e_{xy} in most of the temperature range. Note also that the temperature dependence of $\Delta\kappa_{xy}$ is significantly different from κ^e_{xy}.

We shall keep in mind that at finite temperature the WF law is not strictly valid. However, the finite-temperature correction does not modify the order of magnitude of the expected electronic thermal conductivity. Moreover, since inelastic scattering damps thermal transport more than the electrical transport, the expected correction to the Lorenz ratio is downward. In copper, such a downward deviation have been observed in the transverse channel of heat and charge transport as well as in the longitudinal ones [37]. Thus, $L_0 \sigma_{xy} T$ gives an upper bound to the expected κ^e_{xy} and we can safely conclude that enhanced THE is not simply due to the introduction of mobile electrons.

The thermoelectric correction to the thermal conductivity

Before discussing the origin of this additional component, we need to distinguish between two thermal conductivities [38]. The first one is defined by the Fourier equation:

$$\vec{J^Q} = -\overline{\kappa} \vec{\nabla T} \tag{1}$$

In presence of thermoelectric phenomena, the transport equations become:

$$\vec{J^e} = \overline{\sigma} \vec{E} - \overline{\alpha} \vec{\nabla T} \tag{2}$$

$$\vec{J^Q} = \overline{\alpha} T \vec{E} - \overline{\kappa'} \vec{\nabla T} \tag{3}$$

where $\overline{\sigma}$ and $\overline{\alpha}$ are the electric and thermoelectric conductivity tensors. Now if the charge current is kept equal to zero ($\vec{J^e} = \vec{0}$), the combination of the two equations would yield:

$$\vec{J^Q} = (\overline{\alpha}\,\overline{\rho}\,\overline{\alpha}\, T - \overline{\kappa'}) \vec{\nabla T} \tag{4}$$

The resistivity tensor is simply the inverse of the conductivity tensor: $\overline{\rho} = \overline{\sigma}^{-1}$. Note that the true Onsager coefficient is $\overline{\kappa'}$ and not $\overline{\kappa}$. Practically, this distinction matters only when the first term on the right hand of Eq. 4 is not negligible compared to the second term, which happens when the thermoelectric figure of merit is sizeable [38].

We have quantified this difference by measuring longitudinal and lateral temperature differences and electric fields in two distinct experiments. In the first, a finite $\vec{J^Q}$ was applied and the $\vec{J^e}$ was kept equal to zero. In the second, a finite $\vec{J^e}$ was injected without $\vec{J^Q}$. This led us to

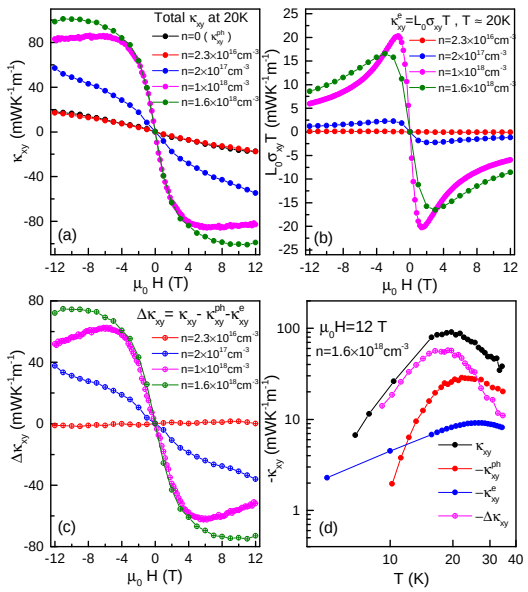

FIG. 2. **Three components of the thermal Hall effect in $SrTiO_{3-\delta}$:** (a) κ_{xy} as a function of magnetic field in samples with different carrier densities at 20 K. With growing metallicity, the amplitude of κ_{xy} increases and its field dependence becomes less linear. (b) Field dependence of the electrical Hall conductivity, σ_{xy}, multiplied by $L_0 = \frac{\pi^2}{3}\frac{k_B^2}{e^2}$, and the temperature, T, in the metallic samples. (c) Field dependence of the differential $\Delta\kappa_{xy} = \kappa_{xy} - \kappa_{xy}(n = 0) - L_0 \sigma_{xy} T$, which signals the presence of a third term in addition to the purely electronic and the purely phononic terms. (d) The evolution of κ_{xy} and its three components as a function of temperature. Below 25 K, $\Delta\kappa_{xy}$ is the largest component.

quantify the diagonal and off-diagonal components of the two conductivities, $\overline{\kappa}$ and $\overline{\kappa'}$. We also checked that the data respect Onsager reciprocity, which implies a unique thermoelectric tensor in equations (2) and (3), (See the supplement for details [39]).

We found that the transverse thermal flow (but not the longitudinal one) is drastically affected by the particle-driven flow of entropy represented by the thermoelectric term (See Fig 3 a). In other words, $\kappa_{xx} \simeq \kappa'_{xx}$, but κ_{xy} and κ'_{xy} are significantly different. The reason is the large Hall angle in the electric and the thermoelectric response. As seen in Fig 3 b, c, the diagonal and off-diagonal components of $\overline{\sigma}$ and $\overline{\alpha}$ are of the same order of magnitude. In contrast, the diagonal component of the thermal conductivity tensor (Fig 3 d) is orders of magnitude larger than the off-diagonal one (Fig 3 e). As a consequence, while the difference between κ_{xx} and κ'_{xx} is of the order of percent (Fig 3 d), κ'_{xy} is 2 times larger than κ_{xy} (Fig 3 e).

Thus, the corrected transverse thermal conductivity is larger than the measured one, which is itself larger than the expected one. The large electric and thermoelectric Hall angles which led to this correction is a key ingredient of the solution to this puzzle. Let us now consider the others.

Discussion

The three ingredients of the scenario

Our scenario invokes three different features of lightly doped strontium titanate. The first is that momentum exchange between phonons and electrons is frequent. Since both the Fermi radius and the phonon thermal wavelength (at our temperature range of interest) are much smaller than the width of the Brillouin zone, such collisions are not Umklapp and conserve momentum. The second feature is that heat is mainly carried by phonons (and not by electrons), $\kappa^e_{xx} \ll \kappa^{ph}_{xx}$, see Fig 4 a). The third is that the Hall angle of electrons exceeds by far the (thermal) Hall angle of phonons. As one can see in Fig 4 b, the phonon thermal Hall angle is 3 orders of magnitude smaller than the electric Hall angle. Lightly-doped strontium titanate is a dilute metal with highly mobile carriers. A moderate magnetic field puts the system in the high field limit, where $\mu B \gg 1$ [40]. The combination of these three features generates an additional thermal Hall response: The longitudinal energy flow, mostly carried by phonons, is accompanied by a flow of electrons and its unavoidable transverse counterpart, which ends up by triggering a phononic transverse flow.

Momentum exchange between electrons and phonons (in presence of heat flow and in absence of charge current) is known as phonon drag [27, 28]. It is known to amplify the thermoelectric response, mostly in semiconductors [27], but also in metals [29]. In the case of strontium titanate, previous studies [41, 42] have shown that phonon drag causes a peak in the zero- field Seebeck coefficient around ~ 20 K. We confirmed the presence of such a peak in our samples (See the supplement [39]). Let us now quantify the expected contribution of phonon drag to transverse thermal transport conductivity.

From Phonon drag to thermal Hall effect

Phonons streaming from hot to cold exert a drag on the charge carriers. To quantify this effect, Herring considered an equivalent phenomenon: the enhancement in the Peltier coefficient of an isothermal sample caused by the drag exerted on phonons by the electric current [27]. Assuming an approximate proportionality between heat current and crystal momentum, he found that a phonon drag Peltier effect, Π_{drag}, of either sign can arise :

$$\Pi_{drag} = \pm \frac{m^* v_s^2}{e} f \frac{\tau_p}{\tau_e} \tag{5}$$

Here, m^* is the effective mass of electrons, v_s is the sound velocity, e is the fundamental charge, τ_p and τ_e are respectively, the phonon and the electron scattering times and $0 < f < 1$ represents the fraction of collisions suffered by phonons, which leads to momentum exchange between the phonon bath and the electron bath. Using the Kelvin relation, the phonon drag component of the Seebeck coefficient becomes Π_{drag}/T. To derive Eq. 5, Herring put forward two arguments. First of all the energy density flux, J^Q, can be approximated by the product of the crystal momentum per unit volume, P and the square of sound velocity, v_s:

$$J^Q = P v_s^2 \tag{6}$$

The second argument is that the rate at which phonons receive crystal momentum from the electronic carriers is to be balanced with the rate at which they lose it. Therefore:

$$\frac{P}{\tau_p} = \pm f n e E \tag{7}$$

Here, n is the carrier concentration, and E is the electric field. The loss of crystal momentum out of the phonon bath is countered by what electrons introduce to this bath. The parameter f is a measure of efficiency of momentum flow between the phonon and electron baths. Herring invoked a 'hydraulic analogy' where momentum first flows from electrons to small q phonons and then distributed among phonons and then eventually lost. In this analogy f plays the role of a half-open valve. Eq.5 can be obtained from Eq.6 and Eq.7, using the Drude link between the electric field and the electric current ($J^e = \frac{ne^2\tau_e}{m^*} E$).

Let us now consider the twist brought by a large Hall angle to this picture. The Peltier phonon drag implies that an electric current can lead to a phonon energy

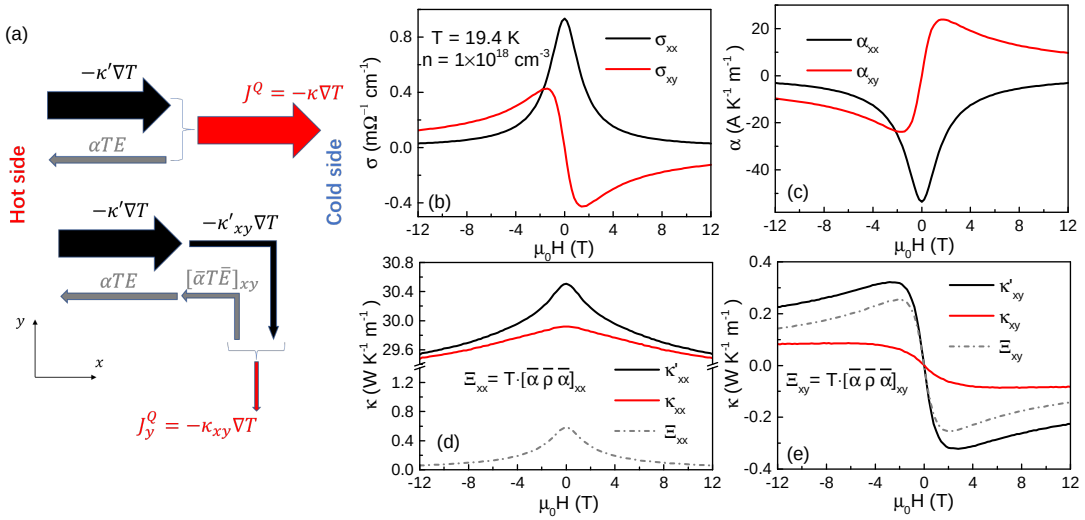

FIG. 3. **The two components of heat flux, :** (a) The heat current density, $\vec{J^Q}$, consists of two terms in both longitudinal and transverse channels. The first component ($-\overline{\kappa}'\vec{\nabla T}$) represents the flow of entropy without particle flow. The second ($\overline{\alpha}T$) is the flow of entropy thanks to particle flow. The difference between κ and κ' is significant when the second term is not negligible. In our case, this happens for the transverse channel. The width of arrows schematize the weight of different components. (b) The longitudinal and the transverse electric conductivity as a function of field at 20 K for $SrTiO_{3-\delta}$ (n=1 $\times$ $10^{18}cm^{-3}$).(c) Same for longitudinal and transverse thermoelectric conductivity . $\overline{\alpha} = \overline{\sigma}\,\overline{S}$. Note that the off-diagonal components rapidly become as large as the diagonal components. (d) κ_{xx} and κ'_{xx} as function of magnetic field. The difference is small. (e) κ_{xy}, κ'_{xy} as function of magnetic field. The difference is significant. Also shown in the panels are the diagonal and the off-diagonal components of the $\overline{\overline{\Xi}} = \overline{\alpha}\,\overline{\rho}\,\overline{\alpha}\,T$ tensor, which quantifies the correction.

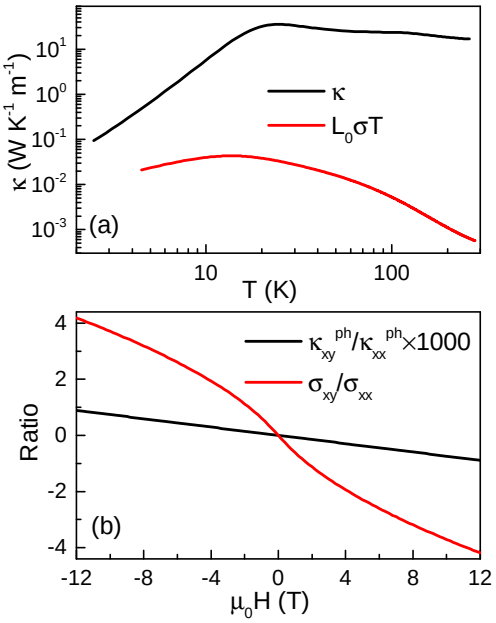

FIG. 4. **Longitudinal thermal conductivity and Hall angles** (a) Thermal conductivity (κ_{xx}) of $SrTiO_{3-\delta}$ ($n = 1 \times 10^{18}cm^{-3}$) as function of temperature and its electronic component ($L_0\sigma T$). Phonons are by far the dominant carriers of heat. (b) The phonon thermal and the electronic Hall angles as the function of field at T= 20 K. The former is three orders of magnitude smaller than the latter.

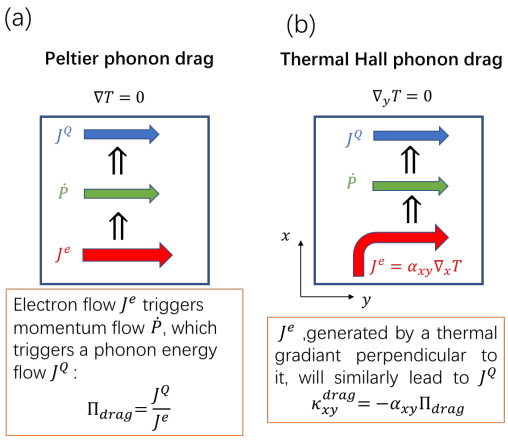

FIG. 5. **From phonon drag to thermal Hall conductivity:** (a) Herring's picture of phonon drag in an isothermal sample. Electronic momentum flow generates a phonon momentum flow which in turn leads to a phonon heat flow. The amplitude of this Peltier effect sets the amplitude of the phonon drag Seebeck effect. (b) Replacing the electronic charge current with a finite transverse thermal gradient multiplied by off-diagonal thermoelectric conductivity quantifies the amplitude of the phonon drag thermal Hall effect.

flow (Fig. 5a). A finite THE driven by phonon drag can be explained in the following way. A finite Nernst-Ettingshausen coefficient implies that a transverse (longitudinal) thermal gradient will generate a longitudinal

(transverse) electric current.Then, this electric current, following Herring's original picture, will generate a thermal current. The latter will be perpendicular to the thermal gradient (Fig. 5b). Therefore, the overall magnitude of this phonon drag THE will be given by the product of the off-diagonal thermoelectric conductivity, α_{xy}, and Herring's expression for Peltier phonon drag:

$$\kappa_{xy}(drag) = \alpha_{xy}\frac{m^* v_s^2}{e} f \frac{\tau_p}{\tau_e} \quad (8)$$

Thus, the component of thermal Hall conductivity generated by mutual drag between electrons and phonons is proportional to the product of α_{xy}, the ratio of phonon and electron scattering times $\frac{\tau_p}{\tau_e}$ and the efficiency of momentum transfer between the two baths, parametrized by f. Let us also note the presence of mv_s^2. This is the kinetic energy of an electron drifting with the velocity of sound, a less familiar energy scale emerging when electrons and phonons couple to each other [43].

Quantitative account of the data

We proceed now to compare $\Delta\kappa_{xy}$ resolved by experiment, with $\kappa_{xy}(drag)$, expected by Eq. 8. With the exception of f, all terms of Eq. 8 are experimentally accessible. The sound velocity is $v_s = 7.8km/s$ [44], the effective mass of electrons is $m^\star = 1.8m_e$ [23]. τ_p can be extracted from phonon thermal conductivity and τ_e from the electrical conductivity.

Fig. 6a shows the non-monotonous field dependence of $\kappa_{xy}(drag)$, which mirrors the field dependence of α_{xy} (Fig. 6b), which, after an initial increase, steadily decreases in the high-field regime. Since $S_{xx} > S_{xy}$ and $\sigma_{xy} \geq \sigma_{xx}$, $\alpha_{xy} \simeq S_{xx}\sigma_{xy}$ and the field dependence of α_{xy}, is similar to the field dependence of Hall conductivity, which steadily decreases in the high-field regime ($\sigma_{xy}(B \longrightarrow \infty) \longrightarrow 0$).

The ratio of τ_p/τ_e, shown on Fig. 6c, is much larger than unity and steadily increases with magnetic field. This is because, as previously documented [40], the mobility of electrons diminishes with magnetic field, presumably because partially extended disorder becomes more effective in scattering electrons with increasing magnetic field which confines the electron wave function. The phonon scattering time on the other hand is barely affected by magnetic field.

By assuming equality between $\Delta\kappa_{xy}$ and $\kappa_{xy}(drag)$ and using Eq. 8, we can extract f. The results are shown in Fig. 6d. We find that $f < 1$, attesting the soundness of our approach. The efficiency of momentum transfer between phonons and electrons is close to 1 at the peak temperature and steadily decreases with temperature. As the temperature decreases, the relative frequency of electron-phonon scattering events decreases. We also note that a strong coupling between electrons and soft ferroelectric phonons has been invoked [45, 46] to explain the transport properties of metallic STO [42, 47]. The steady field-induced decrease in f indicates that the efficiency of the momentum transfer between phonons and electrons decreases with the decrease in the electronic scattering time and the growing mismatch between the phonon and the electron scattering time.

The soundness of our diagnostic can be checked by comparing the extra thermal Hall effect and the phonon drag Seebeck effect, supposed to share the same origin. Both effects, measured by distinct experiments, peak around 20 K. Their amplitude match too. Eq.5 and Eq.8 together with the Kelvin relation ($\Pi = ST$) and the identification of $\Delta\kappa_{xy}$ with $\kappa_{xy}(drag)$ implies an equality between the two extracted quantities: $\Delta\kappa_{xy} \approx -\alpha_{xy}S_{drag}T$. Fig. 6 f compares $\Delta\kappa_{xy}$ and $-\alpha_{xy}\cdot S_{drag}\cdot T$ as a function of temperature at 4 T. The agreement between 25 K down to 10 K confirms the quantitative self-consistency of the data. The disagreement at 5 K indicates the limits of our approximations when f strongly varies with magnetic field.

Relevance to other metallic solids

Our result implies that the combination of phonon-drag (frequently encountered in semiconductors) and a sizeable transverse thermoelectric conductivity, α_{xy} (known to become large when the carrier density is low density and carrier mobility is high[48]) can give rise to a phonon-drag THE. These conditions can be formulated in term of a hierarchy of time scales. The scattering time of phonons should exceed the scattering time of electrons and the latter should in turn exceed the inverse of the cyclotron frequency, in order to ensure longitudinal-to-transverse conversion. Thus, a sizeable phonon drag THE requires:

$$\tau_p > \tau_e > \omega_c^{-1} \quad (9)$$

The second condition is that the rate of momentum lost by phonons is to be comparable to the rate of phonon-electron exchange :

$$f \gg 0 \quad (10)$$

Note that the latter condition can only be satisfied at finite temperature. The hydrodynamic window, identified by Gurzhi [30] requires a hierarchy of time scales too: The momentum-conserving scattering time should outweigh the boundary scattering time, itself larger than the momentum-relaxing scattering time. As a result, hydrodynamic features are expected in a limited temperature window and in a limited number of materials.

Inequalities 9 and 10 specify the conditions for expecting a phonon drag THE. Long τ_p is expected in a crystal at low temperature when phonon wavelength is long and point defects cannot scatter them. In many dilute metals, when the Bohr radius of the semiconducting parent is long [49] carriers are more mobile than in metallic silicon. As a consequence, the inequality $\tau_e > \omega_c^{-1}$ is easily

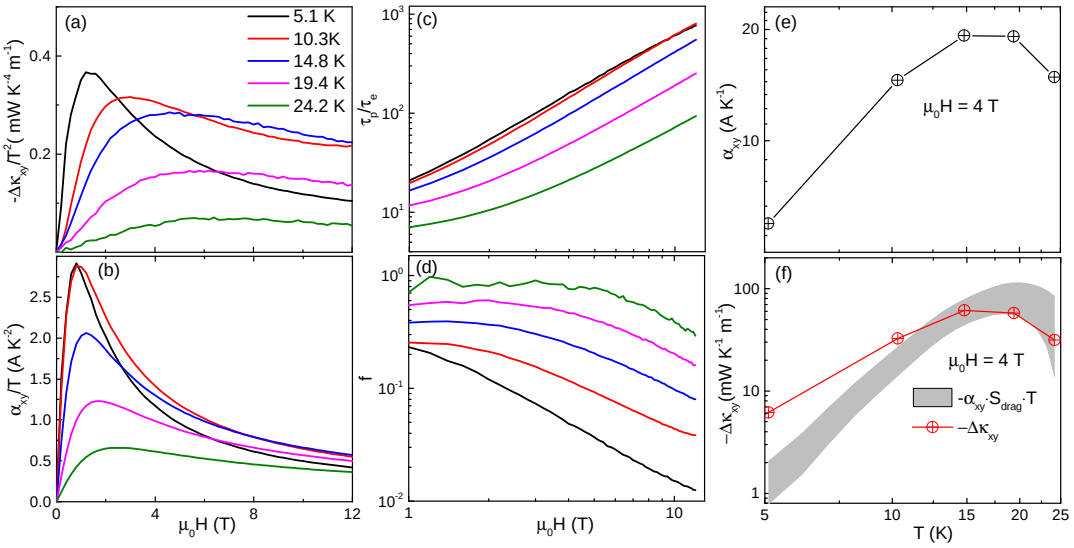

FIG. 6. **Quantitative analysis of $\Delta\kappa_{xy}$:** (a) Field dependence of $\Delta\kappa_{xy}/T^3$ at different temperatures. (b) Field dependence of α_{xy}/T at different temperatures. In our picture, this is the main driver of the field dependence of $\Delta\kappa_{xy}$ (c) Field dependence of the ratio of the phonon to electron scattering time, extracted from electric and thermal conductivity data. Note that $\tau_P \gg \tau_e$ and the ratio enhances with magnetic field. (d) The field dependence of f, obtained by equating $\Delta\kappa_{xy}$ and $\kappa_{xy}(drag)$ given by Eq. 8. (e), The temperature dependence of α_{xy} at 4 T. (f) The temperature dependence of $-\Delta\kappa_{xy}$ and $-\alpha_{xy}S_{drag}\cdot T$. The width of the latter represents the uncertainty in separating the phonon-drag and the diffusive components of the Seebeck coefficient (see the supplement [39]).

satisfied at low fields. If electron-phonon momentum exchange happens to be frequent too, then an effect similar to the one observed here is expected. Possible candidates are Bi_2Se_3 [50], InAs [51], PbTe [52] and their sister compounds. It is not surprising that the thermal Hall effect in metallic cuprates is not detetectably amplified by phonon drag [3]. In their case the mobility of carriers in cuprates is low and, as a consequence, condition 9 is not satisfied. Indeed, the measured Hall angle in $La_{1-x}Sr_xCuO_4$ is quite small. At B=10 T, $\sigma_{xy}/\sigma_{xx} \ll 0.1$ [53] and therefore $\omega_c\tau_e < 1$.

The result reported here does not provide a direct solution to the puzzle of phonon thermal Hall effect in insulators. Nevertheless, the complicity between two types of heat carriers, one with a long scattering time (here phonons) and another with a large Hall angle (here electrons) may have relevance to other contexts. One can imagine a scenario close to ours in an insulating solid hosting two types of carriers: ordinary phonons with a long scattering time and magnons or chiral phonons or with a short scattering time and a large transverse response.

[1] K. Sugii, M. Shimozawa, D. Watanabe, Y. Suzuki, M. Halim, M. Kimata, Y. Matsumoto, S. Nakatsuji, and M. Yamashita, Thermal Hall effect in a phonon-glass $Ba_3CuSb_2O_9$, Phys. Rev. Lett. **118**, 145902 (2017).

[2] Y. Kasahara, K. Sugii, T. Ohnishi, M. Shimozawa, M. Yamashita, N. Kurita, H. Tanaka, J. Nasu, Y. Motome, T. Shibauchi, and Y. Matsuda, Unusual thermal Hall effect in a kitaev spin liquid candidate $\alpha-RuCl_3$, Phys. Rev. Lett. **120**, 217205 (2018).

[3] G. Grissonnanche, A. Legros, S. Badoux, E. Lefrançois, V. Zatko, M. Lizaire, F. Laliberté, A. Gourgout, J.-S. Zhou, S. Pyon, T. Takayama, H. Takagi, S. Ono, N. Doiron-Leyraud, and L. Taillefer, Giant thermal Hall conductivity in the pseudogap phase of cuprate superconductors, Nature **571**, 376 (2019).

[4] Y. Hirokane, Y. Nii, Y. Tomioka, and Y. Onose, Phononic thermal Hall effect in diluted terbium oxides, Phys. Rev. B **99**, 134419 (2019).

[5] X. Li, B. Fauqué, Z. Zhu, and K. Behnia, Phonon thermal Hall effect in strontium titanate, Phys. Rev. Lett. **124**, 105901 (2020).

[6] J. A. N. Bruin, R. R. Claus, Y. Matsumoto, N. Kurita, H. Tanaka, and H. Takagi, Robustness of the thermal Hall effect close to half-quantization in a field-induced spin liquid state (2021), arXiv:2104.12184 [cond-mat.str-el].

[7] É. Lefrançois, G. Grissonnanche, J. Baglo, P. Lampen-Kelley, J. Yan, C. Balz, D. Mandrus, S. E. Nagler, S. Kim, Y.-J. Kim, N. Doiron-Leyraud, and L. Taillefer, Evidence of a Phonon Hall Effect in the Kitaev Spin Liquid Candidate α-$RuCl_3$, arXiv e-prints , arXiv:2111.05493 (2021), arXiv:2111.05493 [cond-mat.str-el].

[8] C. Collignon, X. Lin, C. W. Rischau, B. Fauqué, and

K. Behnia, Metallicity and superconductivity in doped strontium titanate, Annual Review of Condensed Matter Physics **10**, 25 (2019).
[9] S. Sim, H. Yang, H.-L. Kim, M. J. Coak, M. Itoh, Y. Noda, and J.-G. Park, Sizable suppression of thermal Hall effect upon isotopic substitution in $SrTiO_3$, Phys. Rev. Lett. **126**, 015901 (2021).
[10] T. Qin, J. Zhou, and J. Shi, Berry curvature and the phonon Hall effect, Phys. Rev. B **86**, 104305 (2012).
[11] J.-Y. Chen, S. A. Kivelson, and X.-Q. Sun, Enhanced thermal Hall effect in nearly ferroelectric insulators, Phys. Rev. Lett. **124**, 167601 (2020).
[12] X.-Q. Sun, J.-Y. Chen, and S. A. Kivelson, Large extrinsic phonon thermal Hall effect from resonant scattering, arXiv e-prints , arXiv:2109.12117 (2021), arXiv:2109.12117 [cond-mat.mes-hall].
[13] B. Flebus and A. H. MacDonald, Charged Defects and Phonon Hall Effects in Ionic Crystals, arXiv e-prints , arXiv:2106.13889 (2021), arXiv:2106.13889 [cond-mat.mes-hall].
[14] H. Guo and S. Sachdev, Extrinsic phonon thermal Hall transport from Hall viscosity, Phys. Rev. B **103**, 205115 (2021).
[15] A. Zabalo, C. E. Dreyer, and M. Stengel, Rotational g factors and Lorentz forces of molecules and solids from density-functional perturbation theory, arXiv e-prints , arXiv:2112.11946 (2021), arXiv:2112.11946 [cond-mat.mtrl-sci].
[16] P. Bhalla and N. Das, Optical phonon contribution to the thermal conductivity of a quantum paraelectric, Journal of Physics: Condensed Matter **33**, 345401 (2021).
[17] S. E. Rowley, L. J. Spalek, R. P. Smith, M. P. M. Dean, M. Itoh, J. F. Scott, G. G. Lonzarich, and S. S. Saxena, Ferroelectric quantum criticality, Nature Physics **10**, 367 (2014).
[18] K. A. Müller and H. Burkard, Srtio$_3$: An intrinsic quantum paraelectric below 4 k, Phys. Rev. B **19**, 3593 (1979).
[19] J. G. Bednorz and K. A. Müller, $Sr_{1-x}Ca_xTiO_3$: An XY quantum ferroelectric with transition to randomness, Phys. Rev. Lett. **52**, 2289 (1984).
[20] V. V. Lemanov, E. P. Smirnova, P. P. Syrnikov, and E. A. Tarakanov, Phase transitions and glasslike behavior in $Sr_{1-x}Ba_xTiO_3$, Phys. Rev. B **54**, 3151 (1996).
[21] M. Itoh, R. Wang, Y. Inaguma, T. Yamaguchi, Y.-J. Shan, and T. Nakamura, Ferroelectricity induced by oxygen isotope exchange in strontium titanate perovskite, Phys. Rev. Lett. **82**, 3540 (1999).
[22] M. A. Carpenter, C. J. Howard, K. Knight, and Z. Zhang, Structural relationships and a phase diagram for $Sr_{1-x}Ca_xTiO_3$ perovskites, Journal of Physics: Condensed Matter **18**, 10725 (2006).
[23] X. Lin, Z. Zhu, B. Fauqué, and K. Behnia, Fermi surface of the most dilute superconductor, Phys. Rev. X **3**, 021002 (2013).
[24] J. Wang, L. Yang, C. W. Rischau, Z. Xu, Z. Ren, T. Lorenz, J. Hemberger, X. Lin, and K. Behnia, Charge transport in a polar metal, npj Quantum Materials **4**, 61 (2019).
[25] J. Engelmayer, X. Lin, F. Koç, C. P. Grams, J. Hemberger, K. Behnia, and T. Lorenz, Ferroelectric order versus metallicity in $Sr_{1-x}Ca_xTiO_{3-\delta}$ ($x = 0.009$), Phys. Rev. B **100**, 195121 (2019).
[26] C. W. Rischau, X. Lin, C. P. Grams, D. Finck, S. Harms, J. Engelmayer, T. Lorenz, Y. Gallais, B. Fauqué, J. Hemberger, and K. Behnia, A ferroelectric quantum phase transition inside the superconducting dome of $Sr_{1-x}Ca_xTiO_{3-\delta}$, Nature Physics **13**, 643 (2017).
[27] C. Herring, Theory of the thermoelectric power of semiconductors, Phys. Rev. **96**, 1163 (1954).
[28] Y. Gurevich and O. Mashkevich, The electron-phonon drag and transport phenomena in semiconductors, Physics Reports **181**, 327 (1989).
[29] D. K. C. MacDonald, *Thermoelectricity : an introduction to the principles* (Dover Publications, 2006).
[30] R. N. Gurzhi, Hydrodynamic effects at low temperature, Soviet Physics Uspekhi **11**, 255 (1968).
[31] A. Jaoui, A. Gourgout, G. Seyfarth, A. Subedi, T. Lorenz, B. Fauqué, and K. Behnia, Formation of an electron-phonon bi-fluid in bulk antimony, arXiv **2105.08408** (2021).
[32] A. Levchenko and J. Schmalian, Transport properties of strongly coupled electron–phonon liquids, Annals of Physics **419**, 168218 (2020).
[33] X. Huang and A. Lucas, Electron-phonon hydrodynamics, Phys. Rev. B **103**, 155128 (2021).
[34] J. Callaway, Model for lattice thermal conductivity at low temperatures, Phys. Rev. **113**, 1046 (1959).
[35] V. Martelli, J. L. Jiménez, M. Continentino, E. Baggio-Saitovitch, and K. Behnia, Thermal transport and phonon hydrodynamics in strontium titanate, Phys. Rev. Lett. **120**, 125901 (2018).
[36] C. W. Rischau, D. Pulmannová, G. W. Scheerer, A. Stucky, E. Giannini, and D. van der Marel, Isotope tuning of the superconducting dome of strontium titanate, Phys. Rev. Research **4**, 013019 (2022).
[37] Y. Zhang, N. P. Ong, Z. A. Xu, K. Krishana, R. Gagnon, and L. Taillefer, Determining the wiedemann-franz ratio from the thermal hall conductivity: Application to cu and $yba_2cu_3O_{6.95}$, Phys. Rev. Lett. **84**, 2219 (2000).
[38] K. Behnia, *Fundamentals of Thermoelectricity* (Oxford University Press, 2015).
[39] See the supplementary material for more details on the samples and measurement methods.
[40] C. Collignon, Y. Awashima, Ravi, X. Lin, C. W. Rischau, A. Acheche, B. Vignolle, C. Proust, Y. Fuseya, K. Behnia, and B. Fauqué, Quasi-isotropic orbital magnetoresistance in lightly doped $SrTiO_3$, Phys. Rev. Materials **5**, 065002 (2021).
[41] T. A. Cain, A. P. Kajdos, and S. Stemmer, La-doped $SrTiO_3$ films with large cryogenic thermoelectric power factors, Applied Physics Letters **102**, 182101 (2013).
[42] C. Collignon, P. Bourges, B. Fauqué, and K. Behnia, Heavy nondegenerate electrons in doped strontium titanate, Phys. Rev. X **10**, 031025 (2020).
[43] C. H. Mousatov and S. A. Hartnoll, Phonons, electrons and thermal transport in planckian high tc materials, npj Quantum Materials **6**, 81 (2021).
[44] W. Rehwald, Anomalous ultrasonic attenuation at the 105°k transition in strontium titanate, Solid State Communications **8**, 607 (1970).
[45] A. Kumar, V. I. Yudson, and D. L. Maslov, Quasiparticle and nonquasiparticle transport in doped quantum paraelectrics, Phys. Rev. Lett. **126**, 076601 (2021).
[46] K. G. Nazaryan and M. V. Feigel'man, Conductivity and thermoelectric coefficients of doped $SrTiO_3$ at high temperatures, Phys. Rev. B **104**, 115201 (2021).
[47] X. Lin, B. Fauqué, and K. Behnia, Scalable T^2 resistivity in a small single-component Fermi surface, Science **349**,

945 (2015).
[48] K. Behnia and H. Aubin, Nernst effect in metals and superconductors: a review of concepts and experiments, Reports on Progress in Physics **79**, 046502 (2016).
[49] K. Behnia, On mobility of electrons in a shallow fermi sea over a rough seafloor, Journal of Physics: Condensed Matter **27**, 375501 (2015).
[50] B. Fauqué, N. P. Butch, P. Syers, J. Paglione, S. Wiedmann, A. Collaudin, B. Grena, U. Zeitler, and K. Behnia, Magnetothermoelectric properties of Bi_2Se_3, Phys. Rev. B **87**, 035133 (2013).
[51] A. Jaoui, G. Seyfarth, C. W. Rischau, S. Wiedmann, S. Benhabib, C. Proust, K. Behnia, and B. Fauqué, Giant seebeck effect across the field-induced metal-insulator transition of inas, npj Quantum Materials **5**, 94 (2020).
[52] Y. I. Ravich, B. A. Efimova, and I. A. Smirnov, *Semiconducting Lead Chalcogenides*, 1st ed., Monographs in Semiconductor Physics 5 (Springer US, 1970).
[53] Y. Ando, Y. Kurita, S. Komiya, S. Ono, and K. Segawa, Evolution of the Hall coefficient and the peculiar electronic structure of the cuprate superconductors, Phys. Rev. Lett. **92**, 197001 (2004).
[54] A. Spinelli, M. A. Torija, C. Liu, C. Jan, and C. Leighton, Electronic transport in doped srtio$_3$: Conduction mechanisms and potential applications, Phys. Rev. B **81**, 155110 (2010).
[55] B. S. de Lima, M. S. da Luz, F. S. Oliveira, L. M. S. Alves, C. A. M. dos Santos, F. Jomard, Y. Sidis, P. Bourges, S. Harms, C. P. Grams, J. Hemberger, X. Lin, B. Fauqué, and K. Behnia, Interplay between antiferrodistortive, ferroelectric, and superconducting instabilities in $Sr_{1-x}Ca_xTiO_3$, Phys. Rev. B **91**, 045108 (2015).
[56] J. M. D. Coey, M. Venkatesan, and P. Stamenov, Surface magnetism of strontium titanate, Journal of Physics: Condensed Matter **28**, 485001 (2016).

Supplemental Material for "Phonon drag thermal Hall effect in metallic strontium titanate"

S1. Samples

$SrTiO_3$ and Ca-doped $SrTiO_3$ single crystals were provided by CrysTech and SurfaceNet GmbH. Oxygen-deficient $SrTiO_3$ samples were obtained by annealing them in a temperature range extending from 700^oC to 1000 ^oC under a high vacuum ($< 10^{-6}$ mbar) for 1 to 2 hours. Fig S1 shows the Hall carrier density of the oxygen-reduced samples as function of the annealing temperature. These results are similar to what was previously reported in oxygen reduced $SrTiO_3$ samples [23, 54].

No.	Supplier	Dimensions (mm)	Peak of κ_{xx} ($W.K^{-1}m^{-1}$)	Peak of κ_{xy} ($mW.K^{-1}.m^{-1}$)	Ca concentration (ppm)
Ref#1 [5]	SurfaceNet	$5 \times 5 \times 0.5$	37	80	3.8
Ref#3 [5]	SurfaceNet	$5 \times 5 \times 0.5$	35	26	2.5
#1	CrysTech	$5 \times 5 \times 0.93$	38.6	21.6	290
#2	SurfaceNet	$5 \times 5 \times 0.5$	34	24	69
#3	SurfaceNet	$5 \times 5 \times 0.5$	32	24	-
#4	CrysTech	$5 \times 5 \times 0.82$	-	3.3	4500
#5	CrysTech	$5 \times 5 \times 0.99$	-	0.6	9100

TABLE S1. Properties of the insulating samples studied in this work. Ca concentration was determined using Secondary Ion Mass Spectrometry (SIMS) and is expressed in part per million (ppm).

The list of the pristine $SrTiO_3$ samples studied in this work, together with their dimensions, the peak amplitude of κ_{xx} and κ_{xy} and their Ca concentration, is shown in Table S1. Ca concentration has been determined using Secondary Ion Mass Spectrometry (SIMS) like in [55].

The amplitude of the κ_{xx} peak is similar in all pristine samples. On the other hand, we found a significant difference in the amplitude of κ_{xy} peak from batch to batch. This variation does not clearly correlate with the amount of residual Ca impurities determined by SIMS. Nominally pristine strontium titanate crystals are known to host other types of impurities such as Fe, O, Ni with a typical concentration of 5 (ppm) [56]. Further studies may find a correlation between the amplitude of the κ_{xy} peak and the concentration of such impurities in nominally pure $SrTiO_3$ samples. In this study all the reduced samples have been prepared from the same batch #3 .

S2. Electric and thermoelectric transport in $SrTiO_{3-\delta}$ samples

Fig.S2 (a) shows the temperature dependence of the resistivity (ρ_{xx}) in $SrTiO_{3-\delta}$ with Hall carrier density (n) ranging from 2.3×10^{16} to $1.6\times10^{18}cm^{-3}$, in good agreement with previous works [47, 54]. Samples with carrier density larger than $10^{17}cm^{-3}$ display a metallic behaviour down to the lowest temperature. In contrast, the lowest

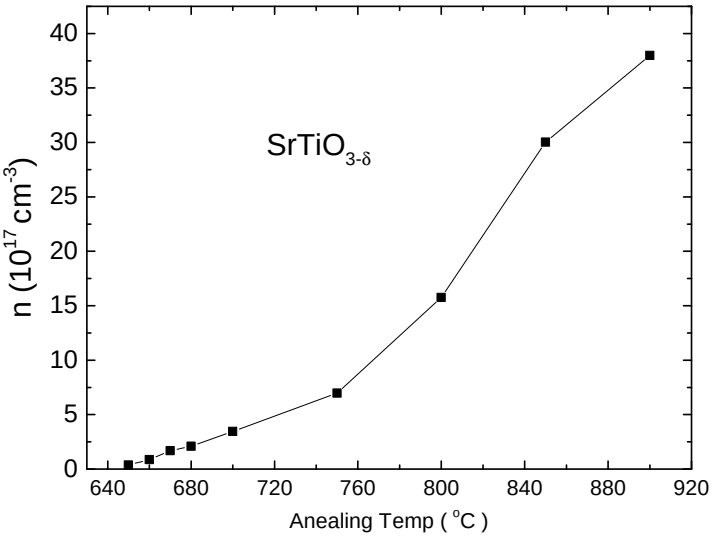

FIG. S1. Carrier density of $SrTiO_{3-\delta}$ as a function of annealing temperature (the vacuum chamber was kept below 10^{-6} mbar).

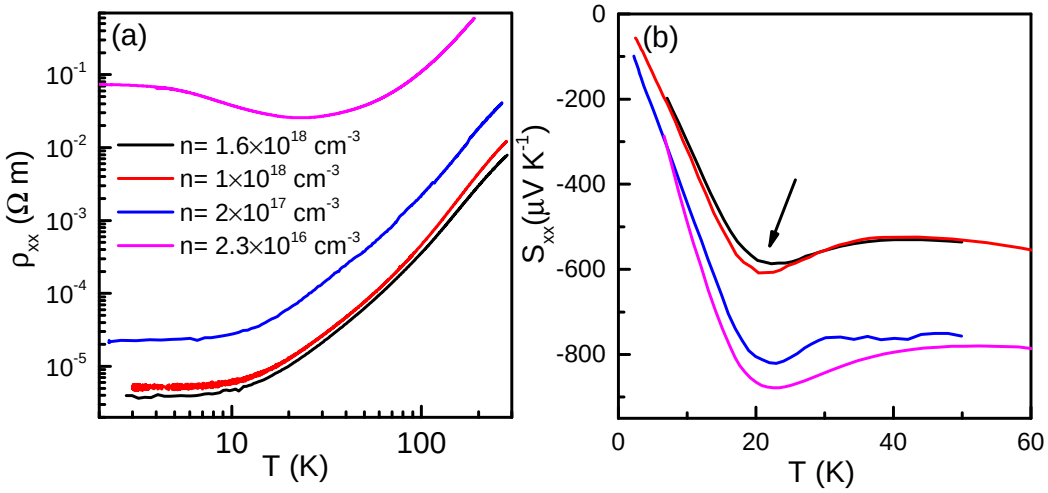

FIG. S2. (a) Resistivity (ρ_{xx}) and (b) Seebeck coefficient (S_{xx}) as function of temperature for $SrTiO_{3-\delta}$ samples with different carrier concentrations. The arrow in (b) indicates the phonon drag peak.

doped sample ($n = 2.3 \times 10^{16} cm^{-3}$) shows an upturn below 30 K, possibly due to inhomogeneous oxygen vacancies distribution or the approach of a genuine metal-insulator transition. This is in agreement with a previous study, which reported an insulating behavior in samples with a carrier density below $n = 3 \times 10^{16} cm^{-3}$ [54].

Fig. S2 (b) shows the temperature dependence of the Seebeck coefficient ($S_{xx} = \frac{E_x}{\Delta_x T}$) in our $SrTiO_{3-\delta}$ samples. S_{xx} peaks around 20 K. This is a signature of phonon drag as discussed below.

Fig. S3 shows the electric properties of $n = 1.6 \times 10^{18}$ sample. The carrier density is determined by measuring the Hall coefficient. The data is similar to what was reported in ref. [40].

S3. Diffusive and phonon drag components of the thermoelectric response

Fig. S4 (a) compares the temperature dependence of S_{xx}/T in doped sample ($n = 1 \times 10^{18}$ cm^{-3}) with previous measurements [23, 41]. Sub-kelvin measurements have shown that S_{xx}/T becomes flat at low temperature (see Fig. S4

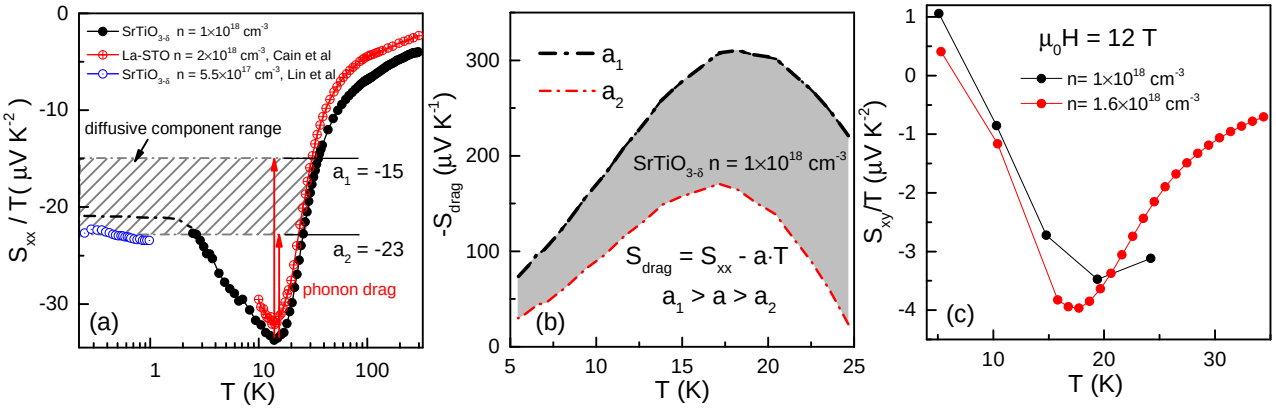

FIG. S3. (a) and (b) ρ_{xx} and ρ_{xy} as function of the magnetic field (B) for T= 5.3 K to 29.8 K.(c) Hall angle ($\frac{\rho_{xy}}{\rho_{xx}}$) *vs.* B.(d) Hall coefficient $R_H = \frac{\rho_{xy}}{B} = \frac{1}{ne}$ *vs.* B.(e) Electron mobility ($\mu = \frac{1}{B} \cdot \frac{\rho_{xy}}{\rho_{xx}}$) *vs.* B.(f) the mean free path of electrons, $l = \tau \cdot v = \frac{\sigma \cdot m^*}{ne^2} \cdot c$ ($m^* = 1.8m_e$ [23] and $c = 3 \times 10^8 m/s$) *vs.* B

(a)) with the expected amplitude for the diffusive response of a degenerate semiconductor with an energy-independent mean free path [23] :

$$|\frac{S}{T}| = \frac{\pi^2}{3}\frac{k_B}{e}\frac{1}{T_F} \tag{S1}$$

T_F is the Fermi temperature, which can be deduced from quantum oscillations. Using Eq.S1 we estimate the amplitude of the diffusive response in our sample with $n = 1 \times 10^{18} cm^{-3}$ to be in the range of $-15 \sim -23\ \mu V K^{-2}$. On top of it, there is a second contribution, the phonon drag (labelled S_{drag}), shown in gray in Fig.S4b). S_{drag} peaks around 20 K, in good agreement with previous work [41]. A similar phonon drag contribution is also detected in the Nernst effect ($S_{xy} = \frac{E_y}{\Delta T_x}$) see Fig. S4 (c).

S4. Verifying Onsager reciprocity

According to the Ohm's law, the electrical field $\vec{E}$ and the charge flux density ($\vec{J^e}$) are linked through the electric conductivity $\overline{\sigma}$:

$$\vec{J^e} = \overline{\sigma}\vec{E} \tag{S1}$$

Similarly, according to the Fourier's law, the thermal conductivity $\overline{\kappa}$ links the thermal gradient $\nabla\vec{T}$ and the heat flux density $\vec{J^Q}$:

$$\vec{J^Q} = -\overline{\kappa}\nabla\vec{T} \tag{S2}$$

The existence of the thermoelectric response modifies both equations:

$$\vec{J^e} = \overline{\sigma'}\vec{E} - \overline{\alpha}\nabla\vec{T} \tag{S3}$$

$$\vec{J^Q} = \overline{\alpha}T\vec{E} - \overline{\kappa'}\nabla\vec{T} \tag{S4}$$

Here $\overline{\sigma'}$, $\overline{\kappa'}$ and $\overline{\alpha}$ are the electric, thermal and thermoelectric conductivity tensors. The thermoelectric contribution in Eq.S3 ($\alpha\nabla T$) and in Eq.S4 (αTE) render $\overline{\sigma}$ and $\overline{\kappa}$ different from $\overline{\sigma'}$ and $\overline{\kappa'}$. In most cases, this contribution to $\overline{\kappa'}$ is negligibly small. However, in our case, this is not true for the transverse component of $\overline{\kappa}$. In other words, $\kappa_{xy} \neq \kappa'_{xy}$.

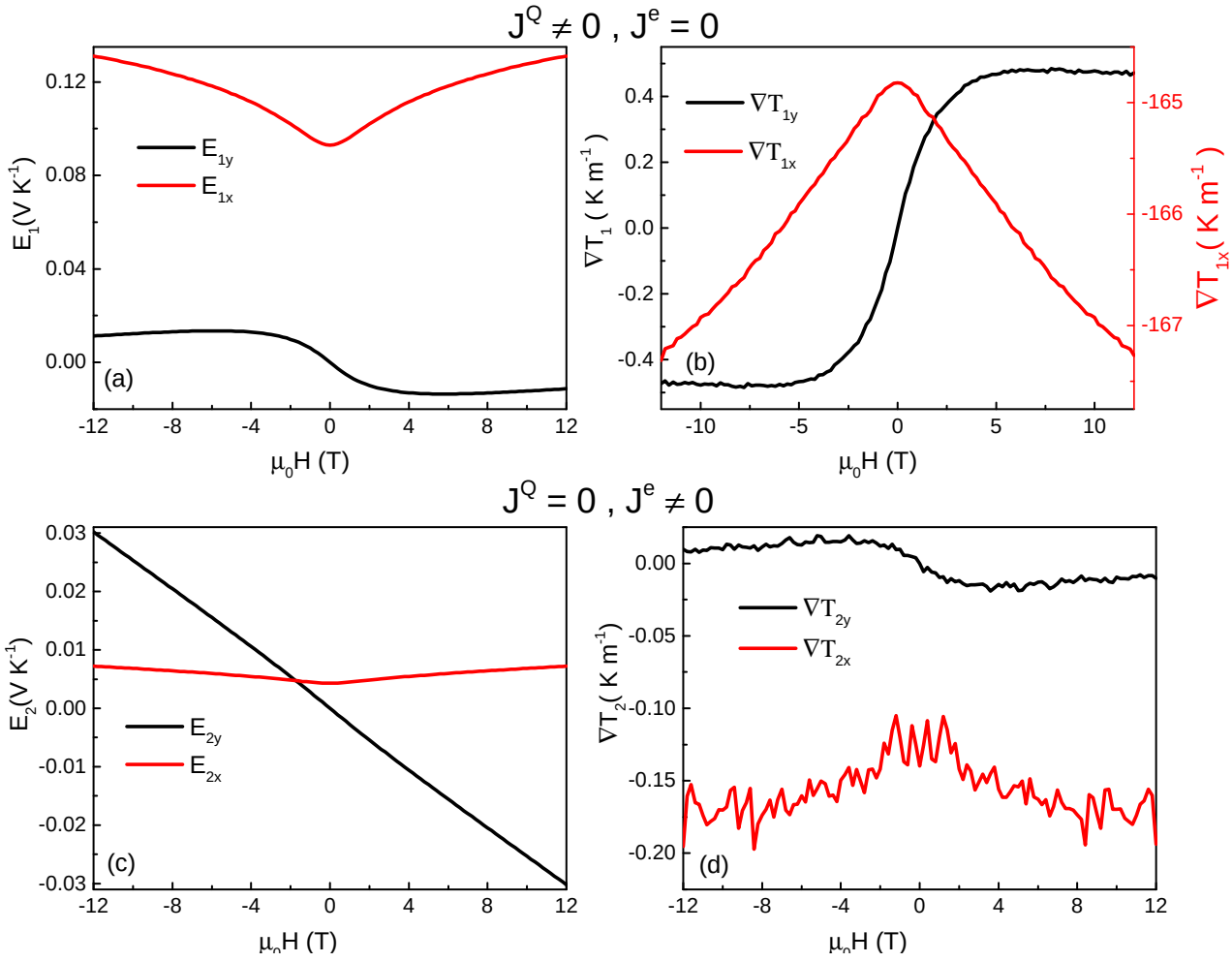

FIG. S4. (a) Temperature dependence of S_{xx}/T in $SrTiO_{3-\delta}$ for n=1× 10^{18} cm^{-3} compared with previous works [23, 41]. The hatched area is the estimated diffusive contribution using Eq.S1. (b) Amplitude of the phonon drag contribution of S_{xx} (gray area) as function of the temperature. $S_{drag} = S_{xx} - a \cdot T$ where $a \cdot T$ is the diffusive contribution shown in (a).(c) Temperature dependence of S_{xy}/T at B= 12 T for n=1× 10^{18} cm^{-3} and 1.6× 10^{18} cm^{-3}. A phonon drag contribution leads to a peaks in S_{xy} around 20 K.

To determine the components of the 2 × 2 tensors $\overline{\sigma'}$, $\overline{\kappa'}$ and $\overline{\alpha}$, we conducted two types of experiments (See Fig. S5 a and d). In the first one, a heat current is applied along the x-axis ($\vec{J^Q} \neq \vec{0}$) and electric current was kept at zero ($\vec{J^e}$=$\vec{0}$). In the second one, an electric current is applied along x axis ($\vec{J^e} \neq \vec{0}$) without heat current ($\vec{J^Q}$=$\vec{0}$). In both experiments, we measured the temperature difference and the electric field along x and y axes at the same time. Fig. S5 b,c and f,g show typical data for both configurations at T= 19.4 K for $SrTiO_{3-\delta}$ (n=1×10^{18} cm^{-3}).

In the first configuration ($\vec{J^Q} \neq 0$ and $\vec{J^e}$=$\vec{0}$), Eq.S3 and Eq.S4 become:

$$\overline{\sigma'}\vec{E_t} = \overline{\alpha}\nabla\vec{T_t} \tag{S5}$$

$$\vec{J^Q} = \overline{\alpha}T\vec{E_t} - \overline{\kappa'}\nabla\vec{T_t} \tag{S6}$$

In the second configuration ($\vec{J^e} \neq 0$ and $\vec{J^Q}$=$\vec{0}$) Eq.S3 and Eq.S4 become:

$$\vec{J^e} = \overline{\sigma'}\vec{E_e} - \overline{\alpha}\nabla\vec{T_e} \tag{S7}$$

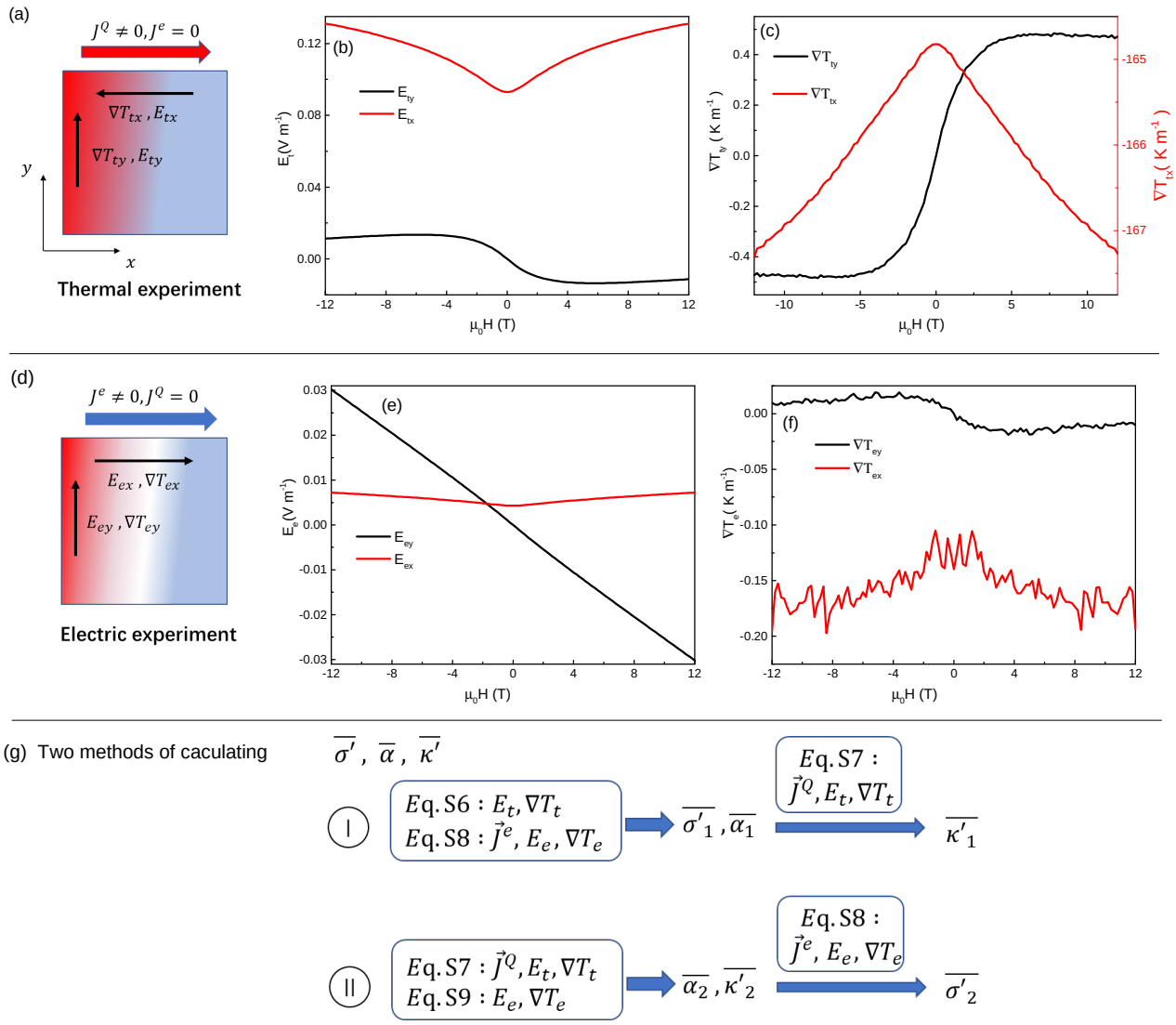

FIG. S5. (a)The first configuration of thermal experiment. (b) Electrical field and (c) thermal gradient measured in $SrTiO_{3-\delta}$ (n=1×10^{18} cm^{-3}) at T = 19.4 K in the thermal experiment ($\vec{J^Q} \neq \vec{0}$ and $\vec{J^e}$=$\vec{0}$). (d)The second configuration of electric experiment. (e) and (f) same as (b) and (c) in the electric experiment ($\vec{J^e} \neq 0$ and $\vec{J^Q}$=$\vec{0}$).(g) Two methods by combining the two configurations to calculate $\overline{\sigma'}$, $\overline{\kappa'}$ and $\overline{\alpha}$.

$$\overline{\alpha} T \vec{E}_e = \overline{\kappa'} \nabla \vec{T}_e \tag{S8}$$

The four equations S5, S6, S7 and S8 projected along the x and y directions give us eight equations to determine six unknown quantities, which are the two components of the three tensors: $\overline{\sigma'} = \begin{bmatrix} \sigma'_{xx} & \sigma'_{xy} \\ -\sigma'_{xy} & \sigma'_{xx} \end{bmatrix}$, $\overline{\alpha} = \begin{bmatrix} \alpha_{xx} & \alpha_{xy} \\ -\alpha_{xy} & \alpha_{xx} \end{bmatrix}$ and $\overline{\kappa'} = \begin{bmatrix} \kappa'_{xx} & \kappa'_{xy} \\ -\kappa'_{xy} & \kappa'_{xx} \end{bmatrix}$ assuming that they are isotropic in the xy plane. The redundancy allows us to make a check on self consistency.

We calculated $\overline{\sigma'}$, $\overline{\alpha}$ and $\overline{\kappa'}$ in two different ways, leading to $\overline{\kappa'}_{1,2}$ and $\overline{\sigma'}_{1,2}$, where the index refers to the set of equations and experimental data used (see Fig S5 (g)). Here, we give explicit expressions for deriving $\overline{\sigma'_1}$ and $\overline{\kappa'_1}$.

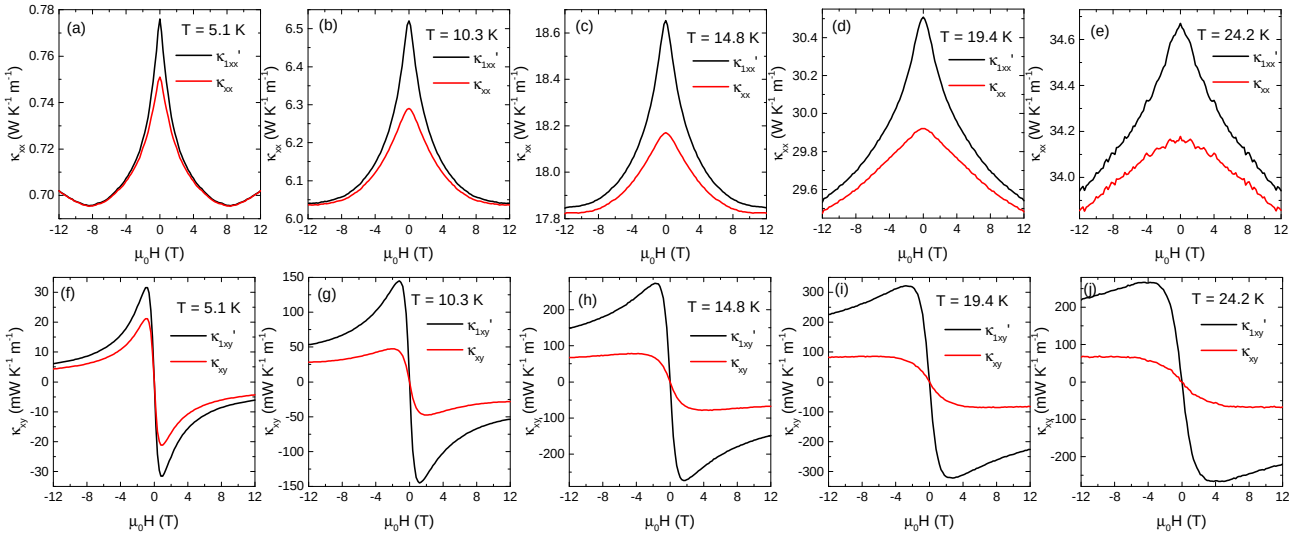

FIG. S6. (a)-(c) Longitudinal electric (σ_{xx}), thermoelectric (α_{xx}) and thermal conductivity (κ_{xx}) as a function of field at T = 19.4 K for $SrTiO_{3-\delta}$ ($n = 1{\times}10^{18}$ cm^{-3}). The black and red colours correspond to two different combinations of Eq. S5, S6, S7 and S8. Black (red) line results were obtained using Eq. S5(S6) S6(S7) and S7(S8). (d)-(f) same as (a)-(c) but for the transverse components of $\overline{\sigma'}$, $\overline{\alpha}$ and $\overline{\kappa'}$.

Starting with Eq. S5 and S7 and setting $S = \sigma^{-1}\alpha$, we obtain :

$$S_{xx} = \frac{E_{tx}\nabla T_{tx} + E_{ty}\nabla T_{ty}}{\nabla T_{tx}^2 + \nabla T_{ty}^2}; S_{xy} = \frac{E_{tx}\nabla T_{ty} - E_{ty}\nabla T_{tx}}{\nabla T_{tx}^2 + \nabla T_{ty}^2} \tag{S9}$$

$$\sigma'^{-1}_{1xx} = \frac{E_{ex} - (S_{xx}\nabla T_{ex} + S_{xy}\nabla T_{ey})}{J^e}; \sigma'^{-1}_{1xy} = \frac{E_{ey} - (-S_{xy}\nabla T_{ex} + S_{xx}\nabla T_{ey})}{-J^e} \tag{S10}$$

$$\alpha_{1xx} = \sigma'_{1xx}S_{xx} - \sigma'_{1xy}S_{xy}; \alpha_{1xy} = \sigma'_{1xx}S_{xy} + \sigma'_{1xy}S_{xx} \tag{S11}$$

Injecting α into Eq. S7, we get $\overline{\kappa'_1}$

$$\kappa'_{1xx} = \frac{[T\cdot(\alpha_{1xx}E_{tx} + \alpha_{1xy}E_{ty}) - J^Q]\cdot -\nabla T_{tx} - T\cdot(-\alpha_{1xy}E_{tx} + \alpha_{1xx}E_{ty})\cdot\nabla T_{ty}}{-\nabla T_{tx}^2 - \nabla T_{ty}^2} \tag{S12}$$

$$\kappa'_{1xy} = \frac{T\cdot(-\alpha_{1xy}E_{tx} + \alpha_{1xx}E_{ty})\cdot\nabla T_{tx} - [T\cdot(\alpha_{1xx}E_{tx} + \alpha_{1xy}E_{ty}) - J^Q]\cdot -\nabla T_{ty}}{-\nabla T_{tx}^2 - \nabla T_{ty}^2} \tag{S13}$$

Method 2 starts with Eq. S6 and S8 and leads to σ'_2, α_2 and κ'_2. Figure S6 compares the results of the two methods. Onsager reciprocity implies no difference because of the identity between the components of the thermoelectric tensor in the two Eq.S3 and S4. Experimentally, we find that this is indeed the case: $\sigma'_{1ij} = \sigma'_{2ij}$; $\alpha'_{1ij} = \alpha'_{2ij}$ and $\kappa'_{1ij} = \kappa'_{2ij}$. Here, i and j refer to x and y orientations and 1 and 2 refer to the method 1 and method 2.

S5. Quantifying the thermoelectric contribution to the thermal conductivity

These measurements allowed us to quantify the thermoelectric contribution to the thermal conductivity. Figure S7 shows the difference between the components of $\overline{\kappa}$ and $\overline{\kappa'}$ at different temperatures. The thermoelectric correction is tiny for the longitudinal thermal conductivity component: $\kappa'_{xx} \approx \kappa_{xx}$ within a percent. On the other hand, it is large for the transverse one: $\kappa'_{xy} \neq \kappa_{xy}$. In other words, the flow of particles carrying entropy with no need for temperature gradient leads to a significant difference in the transverse channel. One can also see that the difference between κ'_{xy} and κ_{xy} decreases with temperature as discussed in the main text.

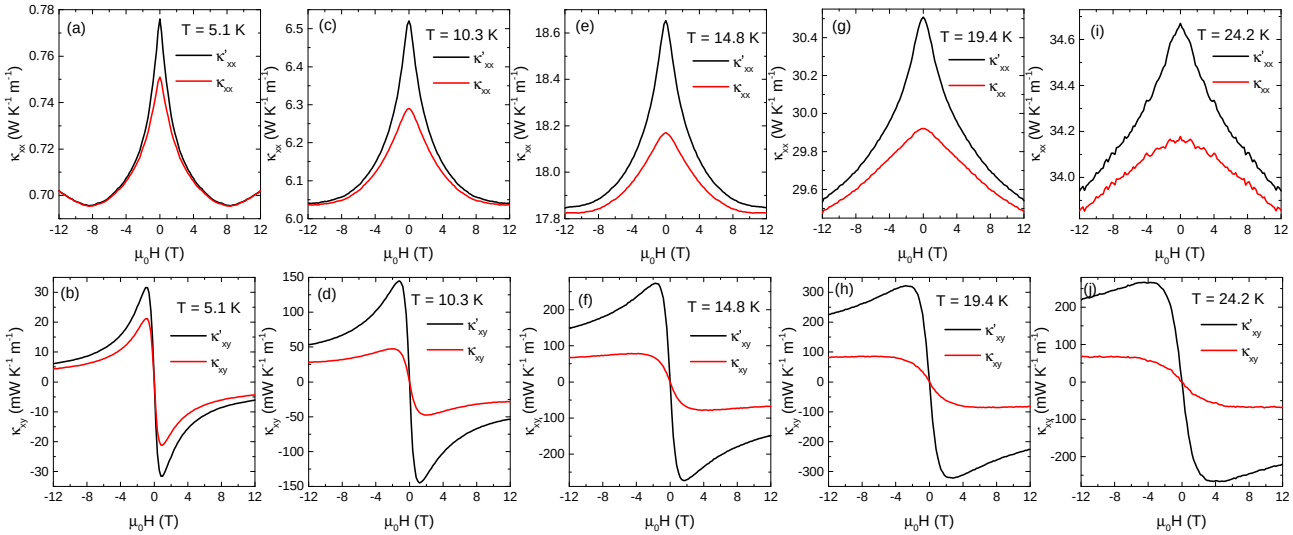

FIG. S7. (a)-(e) Field dependence of κ_{xx} and κ'_{xx} for different temperature in $SrTiO_{3-\delta}$ (n=1×10^{18} cm^{-3}). (f)-(j) Same as (a)-(e) for κ_{xy} and κ'_{xy}.